Thermal Science and Engineering (2023) Volume 6 Issue 2
doi: 10.24294/tse.v6i2.2595

ORIGINAL RESEARCH ARTICLE

Radiation heat transfer of hybrid nanofluid stagnation point flow across a stretching porous cylinder

Ziad Khan[1], Rashid Jan[2,*], Muhammad Jawad[3], Fawad Hussain[1]

[1] *Department of Mathematics, Abbottabad University of Science and Technology, Abbottabad 22500, Pakistan*

[2] *Institute of Energy Infrastructure (IEI), Department of Civil Engineering, College of Engineering, Universiti Tenaga Nasional (UNITEN), Putrajaya Campus, Jalan IKRAM-UNITEN, Kajang 43000, Selangor, Malaysia*

[3] *Department of Mathematics, University of Swabi, Swabi 23561, Khyber Pakhtunkhwa, Pakistan*

*** Corresponding author:** Rashid Jan, rashid.jan@uniten.edu.my

ABSTRACT

The current study provides a comprehensive analysis of MHD hybrid nanofluids and stagnation point flow toward a porous stretched cylinder in the presence of thermal radiation. Here, alumina (Al_2O_3) and copper (Cu) are considered the hybrid nanoparticles, while water (H_2O) is the base fluid. To begin, the required similarity transformations are applied to transform the nonlinear coupled PDEs into nonlinear coupled ODEs. The obtained highly nonlinear sets of ODEs are then solved analytically by using the HAM procedure. The calculations of the thermal radiation term in the energy equation are done based on the Roseland approximation. The result of various embedded variables on temperature and velocity profiles is drawn and explained briefly. Aside from that, the numerical solution of well-known physical quantities, like skin friction and the Nusselt number, is computed by means of tables for the modification of the relevant parameter. The analysis shows that the magnetic field has opposite behavior on $\theta(\eta)$ and $f'(\eta)$ profiles. It is seen that more magnetic factors M decline $f'(\eta)$ and upsurge $\theta(\eta)$. Moreover, the behavior of skin friction and the Nusselt number are the same for the magnetic parameter M. Meanwhile, a higher Reynolds number R_e declines temperature profile and skin friction while upsurging the local Nusselt number. There are many applications of this study that are not limited to engineering and manufacturing, such as polymer industry, crystal growth, tumor therapy, plasma, fusing metal in electric heaters, nuclear reactors, asthma treatment, gastric medication, cooling of atomic systems, electrolytic biomedicine, helical coil heat exchangers, axial fan design, polymer industry, plane counter jets, and solar collectors.

Keywords: hybrid nanofluid; stagnation point flow; thermal radiation; porous stretching cylinder

ARTICLE INFO

Received: 15 August 2023
Accepted: 14 September 2023
Available online: 6 November 2023

1. Introduction and motivation

Many scientists and researchers have long been interested in the work of heat transfer improvement due to boundary layer flow and its impact on thermal conductivities, heat capacities, and other physical characteristics. Nanofluids have drawn significant interest from scientists owing to their ability to motivate heat transfer in a variety of engineering and manufacturing applications. Water, motor oils, and ethylene glycol are examples of traditional working fluids with a low thermal conductivity that limits their usage in modern cooling applications. Nanofluids are made up of nanoparticles, including metal oxide, carbon nanotubes, copper, alumina, and carbides, that enhance the thermal capacity of the base fluid. These nanofluids are utilized in contemporary cooling and heating systems, solar panels, cancer therapy, and drug delivery systems. First, in 1995, Choi and Eastman[1] developed the nanofluid term and discovered that nanofluids have

greater thermal conductivity than base fluid. Sheikholeslami et al.[2] explore the behavior of hydrothermal nanofluid with an electric field effect toward a complicated geometry. Hamad et al.[3] investigated the free convective flow of a nanofluid through vertical semi-infinite flat plates with the impact of magnetic fields. MHD is the study of the magnetic impact of an electrically conducted incompressible fluid; it has received attention because of its major applications in different areas, such as X-ray radiation, crystal growth, asthma treatment, tumor therapy, plasma, fusing metal in electric heaters, nuclear reactors, gastric medication, and electrolytic biomedicine. MHD fluid can also be used to manage cooling rates in certain industrial processes. Khan et al.[4] discussed the analysis of steady 2D boundary layer MHD nanofluid flow toward a thin needle. After the Huminic[5] study, hybrid nanofluids, which contain very small particles with a size of less than 100 nm, have emerged as a new class of working fluid and are useful in applications such as air conditioner units, microchannels, drug reduction, helical coil heat exchangers, cooling of the atomic system, mini channel heat sinks, and cooling of the transformer. The literature contains a wealth of information on hybrid nanofluid. For example, Gabli et al.[6] investigate the influence of Fe_3O_4 nanoparticles in non-Newtonian fluids to improve heat transmission. Sundar et al.[7] examine the higher temperature conversion and friction characteristics of the hybrid nano-liquid. The different features of convective hybrid nano liquids for laminar flow in a tending cylinder are analytically studied by Momin[8]. Later on, many researchers[9–16] discussed the impact of various nanoparticles on different models of fluid.

Stagnation point flow is an essential and important aspect of fluid mechanics. The stagnation point generally occurs in both engineering and science flow fields. The stagnation point region offers the highest mass deposition, pressure, and heat transfer rates. A stagnation point in a flow stream is a position in which the velocity of the fluid is zero while the pressure gradients are large. As a result, it has a variety of applications, including cooling electronic devices, nuclear reactor cooling, polymer extrusion, axial fan design, the polymer industry, plane counter jets, and plastic sheet drawing. Oztop and Abu-Nada[17] were the first researchers to suggest the concept of stagnation flow, where they simplified the Navier-Stokes equation into nonlinear ODEs by using the similarity transformation. After that, in 1936, Homann[18] found the exact solutions of axisymmetric stagnation point flow. The Homann problem toward incompressible viscous fluids approaching the rigid surface for a non-axisymmetric flow is generalized by Weidman[19]. Jawad et al.[20] examined the analysis of hybrid nanofluid and stagnation point flow across a stretching sheet along with melting heat transfer. The Darcy-Forchheimer laminar thin film flow with heat transfer and MHD flow toward an unsteady stretching surface has been analyzed by Khan et al.[21]. The effect of buoyancy on 3D stagnation point flow has been deliberated by Borrelli et al.[22]. According to them, buoyancy forces favor an opposing flow. The numerical solution of nonlinear coupled ODEs using the Runge Kutta 4^{th} order (RK4) method for a steady viscous fluid toward a stagnation point is investigated by Grosan et al.[23]. Wang[24–26] examines the 3D stagnation point flow in the presence of MHD and nanofluid toward a flat plate, rotating, and shrinking disk. Ahmad et al.[27] study the radiation heat transfer influence of copper and alumina nanoparticles toward a stagnation region. The result of homo-heterogeneous reactions and magnetic field toward a stagnation point MHD flow past a shrinking or stretching sheet is considered by Anuar et al.[28]. They observed that two solutions are visible for shrinking sheets, and one of them is stable based on the analysis of stability. Sreekala et al.[29] explore the numerical solution of steady 2D MHD nanofluids and viscous flow toward a stretched surface in the presence of partial slip and thermal radiation. Jawad et al.[30] have reported a 3D electrically incompressible, unsteady rotating single-wall carbon nanotube with thermal radiation. They also examine the numerical results of MHD Darcy-Forchheimer laminar flow toward a permeable surface in the presence of short and Dufour impacts[31]. Many researchers[32–38] perform research on MHD stagnation point flow for different fluids modeled.

Many engineering functions of convection flow in a porous medium have been deliberated in the last few years, including building construction, temperature exchangers, solar collectors, ventilation, and heat removal from nuclear reactors. The heat transfer rate of radiation and buoyancy effect on free convection boundary

layer MHD flow toward a porous stretching sheet have been studied by Srivastava et al.[39]. The continuous flow of fluids across a stretched cylinder as an outer surface was predicted by Wang[40]. Butt et al.[41] studied the combined impact of entropy-generating flow across a stretched cylinder in the continuations of a porous medium; they found that the rise in permeability and magnetic parameters diminishes the thickness of momentum boundary layers. More recently, the researchers[42] discussed the solution of hydrodynamic force in a grooved channel with two partially heated circular cylinders. Many researchers have investigated the deformable cylinder, either shrinking or stretching, because of its extensive application in the engineering area. Abbas et al.[43] calculated the heat transmission rate of viscous fluid in an unstable shrinking/stretching cylinder. Abaszadeh et al.[44,45] analyzed the radiative heat transfer rate in 2-dimensional irregular geometries by applying the direct forcing immersed boundary lattice Boltzmann method. Atashafrooz et al.[46] simulated the combined convective radiative heat transfer for MHD hybrid nanofluid flow. Al Sakkaf et al.[47] developed a computational approach for solving nonlinear BVPs involving fluid flow across a shrinking, porous, unbounded cylinder. The impact of rotation and transpiration on stagnation flow toward a circular cylinder has been examined in the work of Cunning et al.[48]. Wan Zaimi et al.[49] examined an unsteady flow toward a shrinking cylinder and discovered that two solutions exist for a particular range of unsteadiness and suction parameters.

The objective of the current study is motivated by the above-mentioned inquiry as well as the wide range of industrial and engineering applications. It has been discovered that heat transfer studies in the past have been done toward a porous cylinder stretching. However, no attempt has yet been made for the stretching of porous cylinders with hybrid nanoparticles and thermal radiation for MHD and stagnation point flow. Therefore, in this study, we have investigated a steady 2D MHD and stagnation point flow toward a stretched porous cylinder with hybrid nanoparticles and thermal radiation. The governing PDEs have been obtained and then transformed into an arrangement of nonlinearly coupled ODEs by using an appropriate similarity transformation. The corresponding ODEs are then solved through HAM in Mathematica software. Results are graphically demonstrated and enlisted in tabular form to report the influence of the involved parameters on the flow field and heat transfer rate. The originality of the model is pointed out as follows:

1) When compared to individual nanofluids, hybrid nanofluids have higher thermal conductivity, mechanical resistance, chemical stability, and physical strength. Therefore, in this study, the $(Al_2O_3 + Cu/H_2O)$ hybrid nanofluids flow toward a stretching porous cylinder for heat transfer is considered.
2) The study of magnetic fields has extensive applications in physics, chemistry, and engineering. Therefore, in the current work, the magnetic fields are imposed on the flow pattern, while the previous work[50] was without the magnetic field.
3) Thermal radiation is an important characteristic in numerous engineering applications, like advanced types of power plants for nuclear rockets, reentry vehicles, and higher-speed flight. Therefore, in this study, the energy equation is extended with the radiation parameter.
4) Unlike any other analytic approach, the HAM allows us a suitable method to achieve the convergence of the solution series, so we applied the HAM approach to the solutions of highly nonlinear equations.
5) By adding the above-mentioned properties, we have preserved the concept of Waini et al.[50].

2. Problem formulation

Consider a steady 2D boundary layer of MHD hybrid nanofluid and stagnation point flow toward a stretched porous cylinder with a radius a, as shown in **Figure 1**. The cylindrical polar coordinates (r, z) are assigned in the radial and axial directions, respectively. On the $z = 0$ plane, the flow of the cylinder is considered to be symmetric, and on the z-axis, it is axisymmetric with the stagnation point at $r = a$ and $z = 0$.

The cylindrical surface velocity is given by $w_s(z) = 2xz$, where the static and stretched cylinders are represented by $x = 0$ and $x > 0$, respectively. Moreover, the velocity of the free stream is chosen as $w_e(z) = 2yz$, where $y > 0$. Further, the surface and ambient temperatures T_s and T_∞ are taken as constants respectively, where $T_\infty < T_s$.

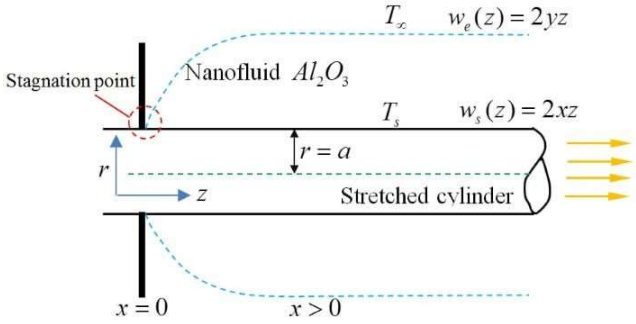

Figure 1. Geometric representation of the physical model for stretching cylinder.

From the above-mentioned supposition, the governing PDEs are as follows:

$$\frac{\partial(ru)}{\partial r} + \frac{\partial(rw)}{\partial z} = 0, \tag{1}$$

$$u\frac{\partial w}{\partial r} + w\frac{\partial w}{\partial z} = w_e\frac{dw_e}{dz} + \frac{\mu_{hnf}}{\rho_{hnf}}\left(\frac{1}{r}\frac{\partial w}{\partial r} + \frac{\partial^2 w}{\partial r^2}\right) - \frac{\sigma_{hnf}}{\rho_{hnf}}\beta_0^2 w - \frac{\mu_{hnf}}{\rho_{hnf}k^*}w, \tag{2}$$

$$\frac{\partial T}{\partial r} + w\frac{\partial T}{\partial z} = \frac{k_{hnf}}{(\rho C_p)_{hnf}}\left(\frac{1}{r}\frac{\partial T}{\partial r} + \frac{\partial^2 T}{\partial r^2}\right) + \frac{\sigma_{hnf}\beta_0^2 w^2}{(\rho C_p)_{hnf}} - \frac{1}{(\rho C_p)_{hnf}}\frac{\partial q_r}{\partial r}. \tag{3}$$

The suitable boundary constraints are as follows:

$$\begin{aligned} &u = 0, \quad w = w_s, \quad T = T_s \quad at \quad r = a \\ &T \to T_\infty, \quad w \to w_e, \quad as \quad r \to \infty. \end{aligned} \tag{4}$$

c

$$q_r = \frac{-\partial T^4}{\partial r}\frac{4\sigma^*}{3k^*}. \tag{5}$$

Here, (k^*) represents the heat absorption coefficient, and (σ^*) is the Stefan-Boltzmann constant with the numerical value $5.670 \times 10^{-8} Wm^{-2}K^4$. The temperature difference is assumed within the flow is T^4 and could be expanded through Taylor's expansion around T_∞ and neglecting higher order than we have $T^4 \approx 4TT_\infty^3 - 3T_\infty^4$.

Hence, Equation (5) can be written as:

$$\frac{\partial q_r}{\partial r} = \frac{-16\sigma^* T_\infty^3}{3(\rho C_p)_f k^*}\frac{\partial^2 T}{\partial r^2}. \tag{6}$$

In order to simplify the present work, we provide a similarity transformation as follows:

$$u = -xaf(\eta)/(\eta)^{\frac{1}{2}}, \quad w = 2xzf'(\eta), \quad \eta = (r/a)^2, \quad \theta(\eta) = \frac{T - T_\infty}{T_s - T_\infty}. \tag{7}$$

Utilizing the above similarity transformation, i.e., Equation (7), into Equations (2) and (3) with boundary conditions, i.e., Equation (4), to get the following dimensionless, higher order nonlinear ODEs:

$$\frac{\mu_{hnf}/\mu_f}{\rho_{hnf}/\rho_f}(\eta f''' + f'') + R_e(ff'' - f'^2 + 1) - \frac{1}{2}\frac{\sigma_{hnf}/\sigma_f}{\rho_{hnf}/\mu_f}Mf' - \frac{1}{\rho_{hnf}}F_1 f'^2 - \frac{1}{2}\frac{\mu_{hnf}}{\rho_{hnf}}k_1 f' = 0, \tag{8}$$

$$\frac{1}{Pr}\frac{1/k_f}{(\rho C_p)_{hnf}/(\rho C_p)_f}\left(\frac{k_{hnf}}{k_f} + \frac{4}{3}Rd\right)\eta\theta'' + \frac{1}{Pr}\frac{k_{hnf}/k_f}{(\rho C_p)_{hnf}/(\rho C_P)_f}\theta' + R_e f\theta' + \frac{\sigma_{hnf}/(\mu\sigma)_f}{(\rho C_P)_{hnf}/(\rho^2 C_p)_f}MEcf'^2 = 0. \tag{9}$$

The related dimensionless form of boundary constraints (BCs) can be defined as:

$$f(1) = 0, \quad f'(1) = \epsilon, \quad f'(\infty) = 1, \quad \theta(1) = 1, \quad \theta(\infty) = 0. \tag{10}$$

Here prime $(')$ denotes differentiation in terms of η, and the stretched parameter is represented by $\epsilon = x/y$ with $0 < \epsilon$, while the cylinder is static by $\epsilon = 0$. The important physical parameters that occur in Equations (8) and (9) are M, Rd, k_1, Pr, and R_e:

$$M=\frac{\sigma\beta_0^2}{\rho_f x},\quad Rd=\frac{4\sigma_0 T_\infty^3}{k^* k_f},\quad k_1=\frac{\mu_f}{\rho_f k^* x},\quad Pr=\frac{\mu_f\left(C_p\right)_f}{k_f},\quad R_e=\frac{xa^2}{2\nu_f}. \tag{11}$$

The two most well-known physical quantities included, C_f and Nu, attract engineers because of their numerous applications in thermodynamics. The dimensionless mathematical expression of these quantities is given as:

$$C_f=\frac{2\tau_s}{\rho_f w_e^2},\quad Nu=\left(1+\frac{16\sigma_0^* T_\infty^3}{3k^* k_f}\right)\frac{aq_s}{k_f(T_s-T_\infty)}. \tag{12}$$

Here q_s and τ_s are the surface heat flux and shear stress which is given as:

$$\tau_s=\mu_{hnf}\left(\frac{\partial w}{\partial r}\right)_{r=a},\quad q_s=-k_{hnf}\left(\frac{\partial T}{\partial r}\right)_{r=a}. \tag{13}$$

Inserting Equations (7) and (13) into Equation (12) we get

$$C_f\left[\frac{R_e}{a}\right]=\frac{\mu_{hnf}}{\mu_f}f''(1),\quad Nu=-2\frac{k_{hnf}}{k_f}\theta'(1)\left(1+\frac{4}{3}Rd\right). \tag{14}$$

3. Thermophysical properties of NF and HNF

The thermophysical properties of hybrid nanofluid and nanofluid are defined in **Table 1**[51,52], while the properties of nanoparticles Al_2O_3, Cu, and H_2O are provided in **Table 2**[52,53].

Here the volume fractions and their solid components are given by ϕ_1, ϕ_2 and t_1, t_2, respectively, for Al_2O_3 and Cu. Moreover, the subscripts f, nf, and hnf are designated for fluid, nanofluid, and hybrid nano-fluid.

Table 1. Physical property of nano fluid and hybrid nanofluid.

Thermophysical characteristics	**Nano fluid**	**Hybrid nanofluid**
Density	$\rho_{nf}=(1-\phi_1)\rho_f+\phi_1\rho_{t_1}$	$\rho_{hnf}=(1-\phi_2)[(1-\phi_1)\rho_f+\phi_1\rho_{t_1}]+\phi_2\rho_{t_2}$
Dynamic viscosity	$\mu_{nf}=\frac{\mu_f}{(1-\phi_1)^{2.5}}$	$\mu_{hnf}=\frac{\mu_f}{(1-\phi_1)^{2.5}(1-\phi_2)^{2.5}}$
Heat capacity	$(\rho C_p)_{nf}=(\rho C_p)_{t_1}\phi_1+(\rho C_p)_f(1-\phi_1)$	$(\rho C_p)_{hnf}=$ $[(1-\phi_1)(\rho C_p)_f+\phi_1(\rho C_p)_{t_1}](1-\phi_2)+(\rho C_p)_{t_2}\phi_2$
Thermal conductivity	$\frac{k_{nf}}{k_f}=\frac{k_{t_1}+2k_f-2\phi_1(k_f-k_{t_1})}{k_{t_1}+2k_f+\phi_1(k_f-k_{t_1})}$	$\frac{k_{hnf}}{k_{nf}}=\frac{k_{t_2}+2k_{nf}-2\phi_2(k_{nf}-k_{t_2})}{k_{t_2}+2k_{nf}+\phi_2(k_{nf}-k_{t_2})}$

Table 2. Property of Al_2O_3, Cu, and H_2O.

Properties	$\boldsymbol{\rho}$ **(kg/m^3)**	$\boldsymbol{k}$ **(W/mK)**	$\boldsymbol{\beta_1\times10^5}$**(1/K)**	$\boldsymbol{C_p}$ **(J/kgK)**
Al_2O_3	3970.0	40.0	0.85	765.0
Cu	8933.0	400.0	1.67	385.0
H_2O	997.10	0.6130	21.0	4179.0

4. Solution procedure through HAM

Many phenomena in the applied science and engineering fields are governed by nonlinear BVPs. As a consequence, BVPs have received a significant concentration from engineers, mathematicians, and physicists for the sake of discovering and studying their solutions. In general, nonlinear ODEs and PDEs are significantly more laborious to solve than linear ODEs and PDEs, particularly by using the analytical method. Therefore, in 1992, Liao[54] proposed the Homotopy Analysis Method HAM[55–60] based on homotopy in topology; this approach is independent of any large or small physical variable. The HAM approach allows great versatility in terms of changing and choosing the convergence area and estimating rates. The method has an advantage over typical computational methodologies in that it avoids rounding off errors induced by the discretization procedure. Therefore, the transformed nonlinear ODEs with the corresponding boundary conditions are solved

through HAM using Mathematica software. The basic derivations of the model equations are presented in the following way:

$$\hat{f}_0(\eta) = e^{-\eta}(e^{-2\eta} + \eta e^{\eta} - \epsilon e + \epsilon e^{\eta}), \quad \hat{\theta}_0(\eta) = e^{1-\eta}, \tag{15}$$

The linearity term is chosen as:

$$L_{\hat{f}}(\hat{f}) = \hat{f}''', \quad L_{\hat{\theta}}(\hat{\theta}) = \hat{\theta}''. \tag{16}$$

The signified linear operator $L_{\hat{f}}$, $L_{\hat{\theta}}$ are fallow as:

$$L_{\hat{f}}(e_1 + e_2\eta + e_3\eta^2) = 0, L_{\hat{\theta}}(e_4 + e_5\eta) = 0, \tag{17}$$

The consistent nonlinear operator $\mathrm{N}_{\hat{f}}$ and $\mathrm{N}_{\hat{\theta}}$ are selected as:

$$\begin{aligned} \mathrm{N}_{\hat{f}}[\hat{f}(\zeta;\eta)] = {} & \frac{\mu_{hnf}/\mu_f}{\rho_{hnf}/\rho_f}(\eta\hat{f}_{\eta\eta\eta} + \hat{f}_{\eta\eta}) + R_e(\hat{f}\hat{f}_{\eta\eta} - \hat{f}_{\eta}^2 + 1) - \frac{1}{2}\frac{\sigma_{hnf}/\sigma_f}{\rho_{hnf}/\mu_f}M\hat{f}_{\eta} \\ & - \frac{1}{\rho_{hnf}}F_1\hat{f}_{\eta}^2 - \frac{1}{2}\frac{\mu_{hnf}}{\rho_{hnf}}k_1\hat{f}_{\eta}, \end{aligned} \tag{18}$$

$$\begin{aligned} \mathrm{N}_{\hat{\theta}}[\hat{f}(\zeta;\eta), \hat{\theta}(\zeta;\eta)] = {} & \frac{1}{Pr}\frac{1/k_f}{(\rho C_p)_{hnf}/(\rho C_p)_f}\left(\frac{k_{hnf}}{k_f} + \frac{4}{3}Rd\right)\eta\hat{\theta}_{\eta\eta} + \frac{1}{Pr}\frac{k_{hnf}/k_f}{(\rho C_p)_{hnf}/(\rho C_P)_f}\hat{\theta}_{\eta} \\ & + R_e\hat{f}\hat{\theta}_{\eta} + \frac{\sigma_{hnf}/(\mu\sigma)_f}{(\rho C_P)_{hnf}/(\rho^2 C_p)_f}MEc\hat{f}^2\eta, \end{aligned} \tag{19}$$

The 0^{th}-Order systems for Equations (8) and (9) are deliberated as:

$$L_{\hat{f}}[\hat{f}(\zeta;\eta) - \hat{f}_0(\eta)](1-\zeta) = p\hbar_{\hat{f}}\mathrm{N}_{\hat{f}}[\hat{f}(\zeta;\eta)], \tag{20}$$

$$L_{\hat{\theta}}[\hat{\theta}(\zeta;\eta) - \hat{\theta}_0(\eta)](1-\zeta) = p\hbar_{\hat{\theta}}\mathrm{N}_{\hat{\theta}}[\hat{f}(\zeta;\eta), \hat{\theta}(\zeta;\eta)]. \tag{21}$$

While BCs are

$$\begin{aligned} & \hat{f}(\zeta;\eta)\big|_{\eta=1} = 0, \quad \left.\frac{\partial\hat{\theta}(\zeta;\eta)}{\partial\eta}\right|_{\eta=1} = \epsilon, \quad \hat{\theta}(\zeta;\eta)\big|_{\eta=1} = 1, \\ & \hat{f}(\zeta;\eta)\big|_{\eta=\infty} = 1, \quad \hat{\theta}(\zeta;\eta)\big|_{\eta=\infty} = 0, \end{aligned} \tag{22}$$

$$\hat{f}(\eta) = \hat{f}(1;\eta), \quad \hat{\theta}(\eta) = \hat{\theta}(1;\eta), \tag{23}$$

$$\hat{f}(\zeta;\eta) = \sum_{n=1}^{\infty}\hat{f}_n(\eta)\zeta^n + \hat{f}_0(\eta), \quad \hat{\theta}(\zeta;\eta) = \sum_{n=1}^{\infty}\hat{\theta}_n(\eta)\zeta^n + \hat{\theta}_0(\eta), \tag{24}$$

$$\hat{f}_n(\eta) = \frac{1}{n!}\left.\frac{\partial\hat{f}(\zeta;\eta)}{\partial\eta}\right|_{p=0}, \quad \hat{\theta}_n(\eta) = \frac{1}{n!}\left.\frac{\partial\hat{\theta}(\zeta;\eta)}{\partial\eta}\right|_{p=0}. \tag{25}$$

While BCs are

$$\hat{f}(1) = 0, \quad \hat{f}'(1) = \epsilon, \quad \hat{\theta}(1) = 1, \quad \hat{f}'(\eta) \to 1, \quad \hat{\theta}(\eta) \to 0 \quad as\ \eta \to \infty \tag{26}$$

$$\begin{aligned} \mathfrak{R}_n^{\hat{f}}(\eta) = {} & \frac{\mu_{hnf}/\mu_f}{\rho_{hnf}/\rho_f}(\eta\hat{f}_{n-1}''' + \hat{f}_{n-1}'') + R_e\left(\sum_{j=0}^{w-1}\hat{f}_{w-1-j}\hat{f}_j'' - \hat{f}_{n-1}'^2 + 1\right) - \frac{1}{2}\frac{\sigma_{hnf}/\sigma_f}{\rho_{hnf}/\mu_f}M\hat{f}_{n-1}' \\ & - \frac{1}{\rho_{hnf}}F_1\hat{f}_{n-1}'^2 - \frac{1}{2}\frac{\mu_{hnf}}{\rho_{hnf}}k_1\hat{f}_{n-1}', \end{aligned} \tag{27}$$

$$\begin{aligned} \mathfrak{R}_n^{\hat{\theta}}(\eta) = {} & \frac{1}{Pr}\frac{1/k_f}{(\rho C_p)_{hnf}/(\rho C_p)_f}\left(\frac{k_{hnf}}{k_f} + \frac{4}{3}Rd\right)\eta\hat{\theta}_{n-1}'' + \frac{1}{Pr}\frac{k_{hnf}/k_f}{(\rho C_p)_{hnf}/(\rho C_P)_f}\hat{\theta}_{n-1}' \\ & + R_e\sum_{j=0}^{w-1}\hat{f}_{w-1-j}\hat{\theta}_j' + \frac{\sigma_{hnf}/(\mu\sigma)_f}{(\rho C_P)_{hnf}/(\rho^2 C_p)_f}MEc\hat{f}_{n-1}^2, \end{aligned} \tag{28}$$

While

$$\chi_n = \begin{cases} 1, & \text{if} \quad n > 1 \\ 0, & \text{if} \quad n \leq 1 \end{cases}. \tag{29}$$

5. Results and discussion

The influences of various physical parameters on velocity $f'(\eta)$ and temperature $\theta(\eta)$ profiles are highlighted in this section through graphical representation. These involved pertinent physical parameters are magnetic parameter M, inertial parameter F_1, porosity parameter k_1, radiation parameter Rd, Reynolds number R_e, Prandtl number Pr and Eckert number Ec. To determine an approximate solution for the dimensionless set of Equations (8) and (9) with boundary conditions as given in Equation (10), we will apply the HAM technique in Mathematica software. The numerical results for physical quantities like skin friction C_f and Nusselt number Nu are presented in tabular form. We took the fixed values of the governing parameters throughout the study as $\mu_{hnf} = 0.5$, $\mu_f = 0.6$, $\sigma_{hnf} = 0.5$, $\sigma_f = 0.6$, $\rho_{hnf} = 0.4$, $\rho_f = 0.3$, $k_{hnf} = 0.3$, $k_f = 0.2$, $(C_P)_{hnf} = 0.7$, $(C_P)_f = 0.4$ and $\epsilon = 0.1$.

5.1. Impact on velocity profile $f'(\eta)$

In this subsection, the impacts of various embedded parameters on the velocity profile $f'(\eta)$ have been studied with the help of a graphical view, as elaborated in **Figures 2–4**. **Figure 2** is plotted to show the behavior of $f'(\eta)$ for different values of magnetic parameter M when $F_1 = 0.2$, $k_1 = 0.5$ and $R_e = 0.7$. It is seen from this figure that an increase in the worth of M decreases $f'(\eta)$. The purpose behind such an influence of M is for the stimulation of a delaying body force, called the Lorentz force, due to the pressure of M in an electrically conducting hybrid nanofluid layer. Since M suggests the ratio of hydro magnetic body force and viscous force, a larger value of M specifies a stronger hydro magnetic body force, which has a tendency to slow the fluid flow. Furthermore, the produced magnetic field upsurges the boundary layer thickness with rise values of M. Physically, it can be deduced that both the applied and induced magnetic fields are going in the same direction. The comparison of a velocity gradient for different amounts of inertial parameter F_1 is visualized in **Figure 3** when $M = 0.4$, $k_1 = 1.2$ and $R_e = 0.6$. From the graph, a decline effect is noticed in $f'(\eta)$ for the upsurge values of the inertia parameter. Physical inertia is the capacity of a mass to resist transitions, therefore, F_1 raises the resistance to precede more powerfully, thus $f'(\eta)$ decreases. The estimations of the porosity parameter k_1 for velocity curves are shown in **Figure 4** when $M = 0.8$, $F_1 = 0.3$, and $R_e = 0.1$. Higher estimations of k_1 lead to decline $f'(\eta)$. Actually, the porosity parameter is inversely proportional to the Darcian drag force that suggested the Darcy number decreases, and hence this is acting to increase the permeability of the fluid flow, which shows to reduce $f'(\eta)$. The improvement of permeability increases the resistive forces within the particle, so that the velocity of the fluids will be diminished.

5.2. Impact on temperature profile $\theta(\eta)$

In this subsection, the impacts of various embedded parameters on the temperature profile $\theta(\eta)$ have been studied with the help of a graphical view, as shown in **Figures 5–9**. **Figure 5** represents the influence of $\theta(\eta)$ for different values of M when $Rd = 1.2$, $Ec = 0.4$, $R_e = 0.8$, and $Pr = 6.7$. It is seen from this figure that the temperature variation increases when the magnetic parameter M values increase. Basically, the existence of a transverse magnetic field creates a Lorentz force that attracts more nanoparticles toward the surface. This Lorentz force has the tendency to slow down the fluid motion and the resistance offered to the flow. Therefore, it is possible for the temperature to increase; hence, the thermal boundary layer thickness increases. Furthermore, the influences of R_e on $\theta(\eta)$ are displayed in **Figure 6** when other parameters are selected as $Rd = 1.2$, $Ec = 1.7$, $M = 0.4$, and $Pr = 6.7$. As predicated, the greater values of R_e decline the temperature field. Physically, the Reynolds number R_e indicates the relative significance of the inertia effect compared to the viscous effect. **Figure 7** highlights the consequence of Pr on $\theta(\eta)$. From the graph, it is observed that by developing Pr with values of 6.7, 6.8, and 6.9, the thermal boundary layers and fluid temperature reduce. This

is because Pr is the ratio of momentum diffusivity, to thermal diffusivity and the thermal diffusivity becomes smaller for higher values of Pr, which decays the temperature and associated boundary layer thickness. Physically, the radiation parameter displays a major role in the progression of heat transmission. Therefore, the influence of Rd on the non-dimensional temperature of the hybrid nanoparticles is demonstrated in **Figure 8**. It is obvious from the graph that the rising values of Rd lead to a release of heat energy in the flow directions, and thus the fluid's temperature increases at any point. The measure of kinetic energy of the flow relative to the enthalpy difference across the thermal boundary layers is known as Eckert number Ec, and the role of Ec in the energy equation is display in **Figure 9**. The upsurge values of Ec rises the temperature field.

5.3. Impact on skin friction C_f and Nusselt number Nu

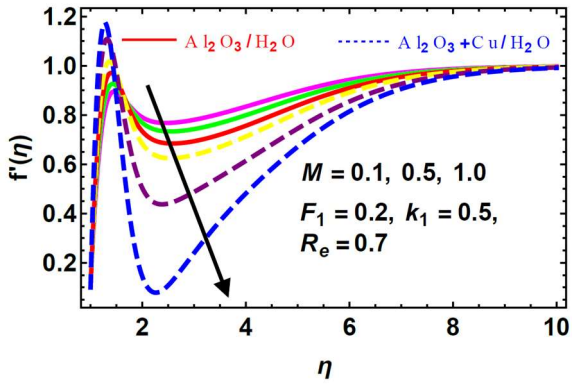

Figure 2. Variation in $f'(\eta)$ for various value of M when $F_1 = 0.2$, $k_1 = 0.5$ and $R_e = 0.7$.

The numerically calculated values have been obtained through a semi analytical method HAM in Mathematica software and are tabulated in **Tables 3** and **4**. The influence of R_e, k_1, M, and F_1 upon C_f is constructed in **Table 3**. The increase in the values of the magnetic parameter rise C_f. This impact is due to rises magnetic factor that upsurge the resistive force on the flow of hybrid nanofluids, known as the Lorentz force. The increasing values of k_1 and F_1 upsurge the skin friction. This is because k_1 (the porosity parameter) disturbs the boundary layer flow of the stretching cylinder, which enhances the resistive force on the hybrid nanofluid. The inertia parameter F_1 is directly proportional to the porosity parameter k_1. The upsurge in the porosity parameter raises the inertia parameter as a result the opposing force to the hybrid nanofluid boosts. More Reynolds number decline C_f. The impact of Rd, M, Pr, Ec, and R_e upon Nu is shown in **Table 4**. It is seen that increases in the values of Rd, Ec, M, and R_e upsurge the Nusselt number Nu, while more values of Pr decline Nu.

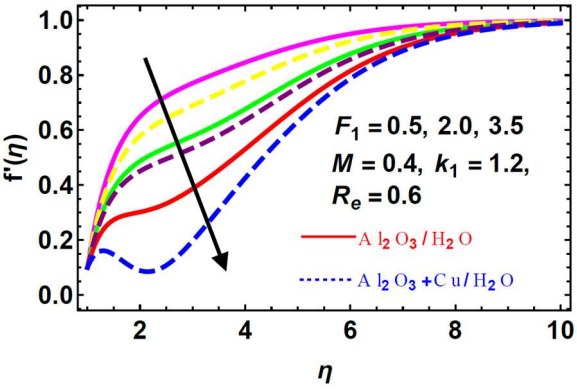

Figure 3. Variation in $f'(\eta)$ for various value of F_1 when $M = 0.4$, $k_1 = 1.2$ and $R_e = 0.6$.

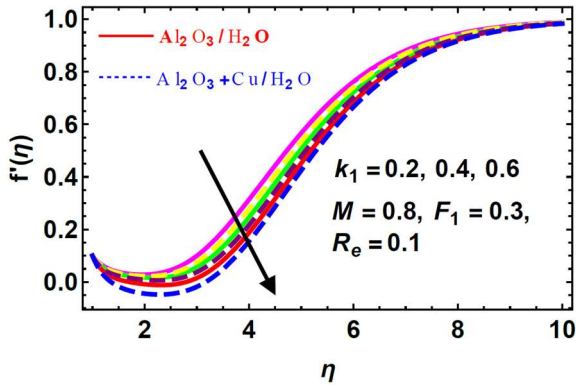

Figure 4. Variation in $f'(\eta)$ for various value of k_1 when $M = 0.8$, $F_1 = 0.3$ and $R_e = 0.1$.

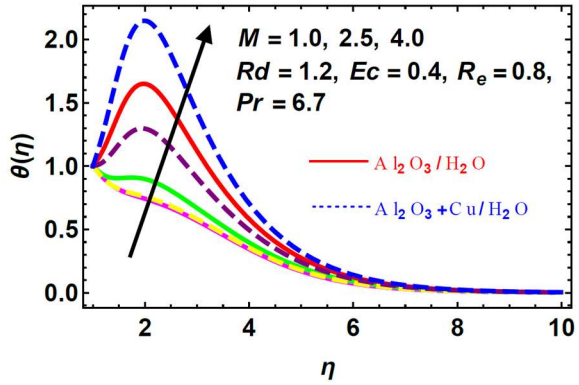

Figure 5. Variation in $\theta(\eta)$ for various value of M when $Rd = 1.2$, $Ec = 0.4$, $R_e = 0.8$ and $Pr = 6.7$.

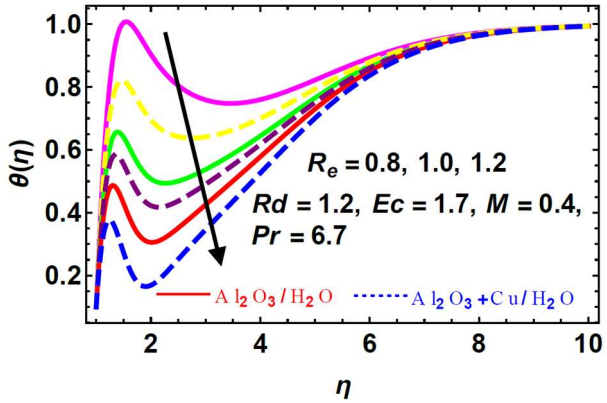

Figure 6. Variation in $\theta(\eta)$ for various value of R_e when $Rd = 1.2$, $Ec = 1.7$, $M = 0.4$ and $Pr = 6.7$.

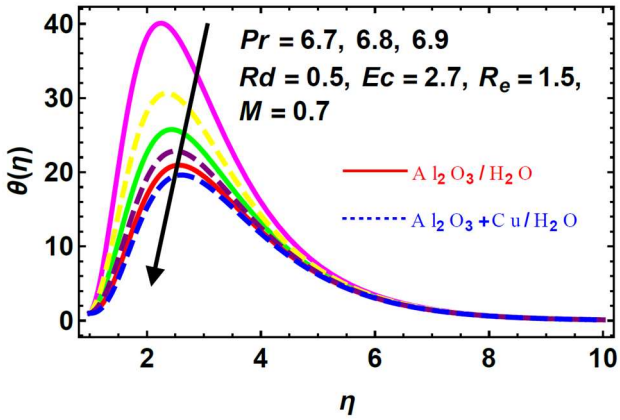

Figure 7. Variation in $\theta(\eta)$ for various value of Pr when $Rd = 0.5$, $Ec = 2.7$, $R_e = 1.5$ and $M = 0.7$.

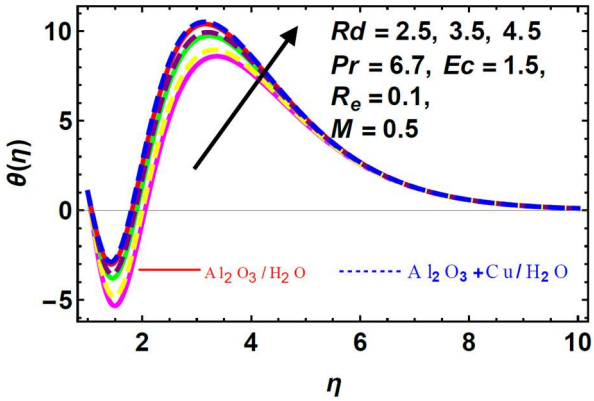

Figure 8. Variation in $\theta(\eta)$ for various value of Rd when $Ec = 1.5$, $Pr = 6.7$, $R_e = 0.1$ and $M = 0.5$.

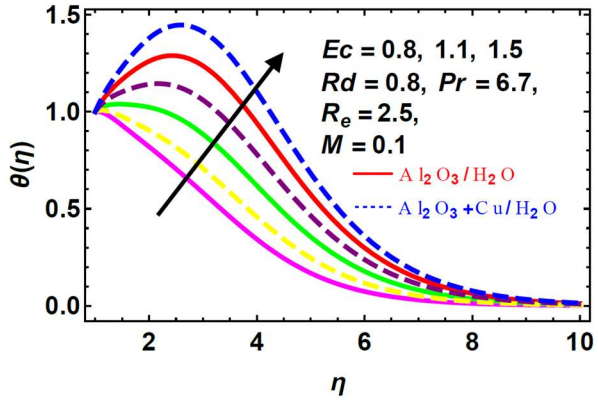

Figure 9. Variation in $\theta(\eta)$ for various value of Ec when $Rd = 0.8$, $Pr = 6.7$, $R_e = 2.5$ and $M = 0.1$.

Table 3. Influence of various embedded parameters upon C_f.

R_e	k_1	M	F_1	C_f
0.8	0.2	0.5	0.3	1.481045028
0.9	-	-	-	1.462384206
1.0	-	-	-	1.440279109
-	0.2	-	-	1.340481045
-	0.3	-	-	1.362275047
-	0.4	-	-	1.382720426
-	-	0.5	-	1.124810286
-	-	0.8	-	1.144602709
-	-	1.0	-	1.153860889
-	-	-	0.3	1.225860022
-	-	-	0.5	1.230290129
-	-	-	0.7	1.250430518

Table 4. Influence of various embedded parameters upon Nu.

Rd	M	Pr	Ec	R_e	Nu
0.3	0.5	5.5	0.8	0.8	1.504237108
0.5	-	-	-	-	1.501025234
0.7	-	-	-	-	1.450345207
-	0.5	-	-	-	1.236410434
-	0.8	-	-	-	1.215302874

Table 4. (*Continued*).

Rd	M	Pr	Ec	R_e	Nu
-	1.0	-	-	-	1.205485159
-	-	5.5	-	-	1.440890179
-	-	5.6	-	-	1.486860828
-	-	5.8	-	-	1.507430387
-	-	-	0.8	-	1.321714801
-	-	-	1.1	-	1.310703405
-	-	-	1.3	-	1.254080658
-	-	-	-	0.8	1.382583605
-	-	-	-	0.9	1.350215207
-	-	-	-	1.0	1.324702164

6. Conclusion

This research work is concerned with emphasizing the problem of MHD hybrid nanofluid and stagnation point flow toward a porous stretched cylinder in the presence of thermal radiation, where the hybrid nanofluid flow is considered the 2-dimensional and steady-state boundary layer. The nanofluid applied in this research work is a mixture of hybrid $Al_2O_3 + Cu$ nanoparticles and base fluid H_2O. The results are obtained through a semi analytical approach HAM in Mathematica software. The effect of various embedded parameters on $f'(\eta)$ and $\theta(\eta)$ is highlighted through graphs. The skin friction C_f and Nusselt number Nu are evaluated through the numerical values presented in tabulated form. The following outcomes can be drawn from this analysis:

- For better estimation of the magnetic field, the distribution of the velocity profile declines while the distribution of the temperature field upsurges.
- More estimation of Reynolds number and Prandtl number reduces temperature $\theta(\eta)$ field.
- The rises values of embedded parameters k_1 and F_1 decline $f'(\eta)$.
- An increase in temperature distributions is observed for a more accurate estimation of Eckert number and radiation parameter.
- Higher estimations of R_e and Pr decline C_f.
- An increase in values M, k_1, and F_1 upsurge C_f, while Nu increases when the values of M, Ec, Rd, and R_e increase.
- The results reveal that hybrid nanofluid is the best capable source to enhance heat transfer rates due to its higher thermal conductivity, mechanical resistance, higher chemical stability and physical strength.

Author contributions

Conceptualization, ZK and RJ; methodology, MJ; software, RJ; validation, ZK, MJ and FH; formal analysis, MJ; investigation, RJ; resources, FH; data curation, RJ; writing—original draft preparation, ZK; writing—review and editing, ZK; visualization, FH; supervision, MJ; project administration, RJ; funding acquisition, RJ. All authors have read and agreed to the published version of the manuscript.

Conflict of interest

The authors declare no conflict of interest.

Nomenclature

r, z	Cylindrical polar coordinates	ρ	Density of fluid (kgm^{-3})

u	Velocity component in term of r-axis	t_1	Solid component of Al_2O_3
w	Velocity component in term of z-axis	C_f	Skin friction
w_e	Free stream velocity (ms^{-1})	μ	Dynamic viscosity of fluid ($kgm^{-1}s^{-1}$)
w_s	Surface velocity (ms^{-1})	σ^*	Stefan-Boltzmann constant
$f(\eta)$	Dimensionless stream function	ρC_p	Heat capacity of fluid ($JKm^{-1}m^{-3}$)
C_p	Specific heat ($Jkg^{-1}K^{-1}$)	k^*	Heat absorption coefficient
k	Thermal conductivity ($Wm^{-1}K^{-1}$)	β_0	Induced magnetic field
ϵ	Stretching parameter	τ_s	Shear stress
Pr	Prandtl number	q_s	Heat flux
R_e	Reynolds number	ϕ_1	Volume fraction for Al_2O_3 nanoparticle
Nu	Nusselt number	ϕ_2	Volume fraction for nanoparticle Cu
Ec	Eckert number	f	Base fluid
M	Magnetic parameter	nf	Nanofluid
Rd	Radiation parameter	hnf	Hybrid nanofluid
k_1	Porosity parameter	η	Similarity variable
T	Temperature of the fluid (K)	t_2	Solid component of Cu
T_s	Surface temperature (K)	T_∞	Ambient temperature (K)
PDEs	Partial differential equations	$f'(\eta)$	Velocity profile
ODEs	Ordinary differential equations	$\theta(\eta)$	Temperature profile
BVPs	Boundary value problems	HAM	Homotopy analysis method
a	Radius of cylinder	MHD	Magnetohydrodynamic

References

1. Choi SUS, Eastman JA. Enhancing thermal conductivity of fluids with nanoparticles. In: Proceedings of the 1995 International Mechanical Engineering Congress and Exhibition; 12–17 November 1995; San Francisco, CA, United States. pp. 99–105.
2. Sheikholeslami M, Soleimani S, Ganji DD. Effect of electric field on hydrothermal behavior of nanofluid in a complex geometry. *Journal of Molecular Liquids* 2016; 213: 153–161. doi: 10.1016/j.molliq.2015.11.015
3. Hamad MAA, Pop I, Md Ismail AI. Magnetic field effects on free convection flow of a nanofluid past a vertical semi-infinite flat plate. *Nonlinear Analysis: Real World Applications* 2011; 12(3): 1338–1346. doi: 10.1016/j.nonrwa.2010.09.014
4. Khan Z, Srivastava HM, Mohammed PO, et al. Thermal boundary layer analysis of MHD nanofluids across a thin needle using non-linear thermal radiation. *Mathematical Biosciences and Engineering* 2022; 19(12): 14116–41141. doi: 10.3934/mbe.2022658
5. Huminic G, Huminic A. Hybrid nanofluids for heat transfer applications—A state-of-the-art review. *International Journal of Heat and Mass Transfer* 2018; 125: 82–103. doi: 10.1016/j.ijheatmasstransfer.2018.04.059
6. Gabli A, Kezzar M, Zighed L, et al. Simultaneous impacts of Fe_3O_4 particles and thermal radiation on natural convection of non-Newtonian Flow between two vertical flat plates using ADM. *Journal of Non-Equilibrium Thermodynamics* 2020; 45(2): 173–189. doi: 10.1515/jnet-2019-0083
7. Sundar LS, Singh MK, Sousa ACM. Enhanced heat transfer and friction factor of MWCNT–Fe_3O_4/water hybrid nanofluids. *International Communications in Heat and Mass Transfer* 2014; 52: 73–83. doi: 10.1016/j.icheatmasstransfer.2014.01.012
8. Momin GG. Experimental investigation of mixed convection with water-Al_2O_3 & hybrid nanofluid in inclined tube for laminar flow. *International Journal of Scientific & Technology Research* 2013; 12(2): 195–202.
9. Bachok N, Ishak A, Pop I. Boundary layer stagnation-point flow and heat transfer over an exponentially stretching/shrinking sheet in a nanofluid. *International Journal of Heat and Mass Transfer* 2012; 55(25–26): 8122–8128. doi: 10.1016/j.ijheatmasstransfer.2012.08.051
10. Merkin JH, Najib N, Bachok N, et al. Stagnation-point flow and heat transfer over an exponentially stretching/shrinking cylinder. *Journal of the Taiwan Institute of Chemical Engineers* 2017; 74: 65–72. doi: 10.1016/j.jtice.2017.02.008
11. Hussain S, Ahmed SE, Akbar T. Entropy generation analysis in MHD mixed convection of hybrid nanofluid in

an open cavity with a horizontal channel containing an adiabatic obstacle. *International Journal of Heat and Mass Transfer* 2017; 114: 1054–1066. doi: 10.1016/j.ijheatmasstransfer.2017.06.135
12. Dhinesh Kumar D, Valan Arasu A. A comprehensive review of preparation, characterization, properties and stability of hybrid nanofluids. *Renewable and Sustainable Energy Reviews* 2018; 81: 1669–1689. doi: 10.1016/j.rser.2017.05.257
13. Sajid MU, Ali HM. Thermal conductivity of hybrid nanofluids: A critical review. *International Journal of Heat and Mass Transfer* 2018; 126: 211–234. doi: 10.1016/j.ijheatmasstransfer.2018.05.021
14. Hemmat Esfe M, Wongwises S, Naderi A, et al. Thermal conductivity of Cu/TiO_2–water/EG hybrid nanofluid: Experimental data and modeling using artificial neural network and correlation. *International Communications in Heat and Mass Transfer* 2015; 66: 100–104. doi: 10.1016/j.icheatmasstransfer.2015.05.014
15. Zadkhast M, Toghraie D, Karimipour A. Developing a new correlation to estimate the thermal conductivity of MWCNT-CuO/water hybrid nanofluid via an experimental investigation. *Journal of Thermal Analysis and Calorimetry* 2017; 129(2): 859–867. doi: 10.1007/s10973-017-6213-8
16. Pourrajab R, Noghrehabadi A, Behbahani M, Hajidavalloo E. An efficient enhancement in thermal conductivity of water-based hybrid nanofluid containing MWCNTs-COOH and Ag nanoparticles: Experimental study. *Journal of Thermal Analysis and Calorimetry* 2021; 143(5): 3331–3343. doi: 10.1007/s10973-020-09300-y
17. Oztop HF, Abu-Nada E. Numerical study of natural convection in partially heated rectangular enclosures filled with nanofluids. *International Journal of Heat and Fluid Flow* 2008; 29(5): 1326–1336. doi: 10.1016/j.ijheatfluidflow.2008.04.009
18. Homann F. The need for high speed in the flow around the cylinder and around the sphere (German). *Zeitschrift fur Angewandte Mathematik und Mechanik* 1936; 16: 153–164. doi: 10.1002/zamm.19360160304
19. Weidman PD. Non-axisymmetric Homann stagnation-point flows. *Journal of Fluid Mechanics* 2012; 702: 460–469. doi: 10.1017/jfm.2012.197
20. Jawad M, Khan Z, Bonyah E, Jan R. Analysis of hybrid nanofluid stagnation point flow over a stretching surface with melting heat transfer. *Mathematical Problems in Engineering* 2022; 2022: 1–12. doi: 10.1155/2022/9469164
21. Khan Z, Jawad M, Bonyah E, et al. Magnetohydrodynamic thin film flow through a porous stretching sheet with the impact of thermal radiation and viscous dissipation. *Mathematical Problems in Engineering* 2022; 2022: 1–10. doi: 10.1155/2022/1086847
22. Borrelli A, Giantesio G, Patria MC. Numerical simulations of three-dimensional MHD stagnation-point flow of a micropolar fluid. *Computers & Mathematics with Applications* 2013; 66(4): 472–489. doi: 10.1016/j.camwa.2013.05.023
23. Grosan T, Pop I, Revnic C, Ingham DB. Magnetohydrodynamic oblique stagnation-point flow. *Meccanica* 2009; 44(5): 565–572. doi: 10.1007/s11012-009-9196-0
24. Wang CY. Stagnation flow on a plate with anisotropic slip. *European Journal of Mechanics—B/Fluids* 2013; 38: 73–77. doi: 10.1016/j.euromechflu.2012.10.005
25. Wang CY. Off-centered stagnation flow towards a rotating disc. *International Journal of Engineering Science* 2008; 46(4): 391–396. doi: 10.1016/j.ijengsci.2008.01.014
26. Wang CY. Stagnation flow towards a shrinking sheet. *International Journal of Non-Linear Mechanics* 2008; 43(5): 377–382. doi: 10.1016/j.ijnonlinmec.2007.12.021
27. Ahmed J, Shahzad A, Farooq A, et al. Radiative heat transfer in Homann stagnation-point flow of hybrid nanofluid. *Applied Nanoscience* 2020; 10(12): 5305–5314. doi: 10.1007/s13204-020-01464-1
28. Anuar NS, Bachok N, Pop I. Cu-Al_2O_3/water hybrid nanofluid stagnation point flow past MHD stretching/shrinking sheet in presence of homogeneous-heterogeneous and convective boundary conditions. *Mathematics* 2020; 8(8): 1237. doi: 10.3390/math8081237
29. Sreekala B, Janardhan K, Ramya D, Shravani I. MHD boundary layer nanofluid flow of heat transfer over a nonlinear stretching sheet presence of thermal radiation and partial slip with suction. *Global Journal of Pure and Applied Mathematics* 2017; 13(9): 4927–4941.
30. Jawad M, Shah Z, Islam S, et al. Impact of nonlinear thermal radiation and the viscous dissipation effect on the unsteady three-dimensional rotating flow of single-wall carbon nanotubes with aqueous suspensions. *Symmetry* 2019; 11(2): 207. doi: 10.3390/sym11020207
31. Jawad M, Saeed A, Kumam P, et al. Analysis of boundary layer MHD Darcy-Forchheimer radiative nanofluid flow with Soret and Dufour effects by means of Marangoni convection. *Case Studies in Thermal Engineering* 2021; 23: 100792. doi: 10.1016/j.csite.2020.100792
32. Khashi'ie NS, Arifin NM, Rashidi MM, et al. Magnetohydrodynamics (MHD) stagnation point flow past a shrinking/stretching surface with double stratification effect in a porous medium. *Journal of Thermal Analysis and Calorimetry* 2020; 139(6): 3635–3648. doi: 10.1007/s10973-019-08713-8
33. Mohd Nasir NAA, Ishak A, Pop I. Stagnation-point flow and heat transfer past a permeable quadratically stretching/shrinking sheet. *Chinese Journal of Physics* 2017; 55(5): 2081–2091. doi: 10.1016/j.cjph.2017.08.023
34. Kamal F, Zaimi K, Ishak A, Pop I. Stability analysis on the stagnation-point flow and heat transfer over a permeable stretching/shrinking sheet with heat source effect. *International Journal of Numerical Methods for Heat & Fluid Flow* 2018; 28(11): 2650–2663. doi: 10.1108/HFF-01-2018-0031

35. Kamal F, Zaimi K, Ishak A, Pop I. Stability analysis of MHD stagnation-point flow towards a permeable stretching/shrinking sheet in a nanofluid with chemical reactions effect. *Sains Malaysiana* 2019; 48(1): 243–250. doi: 10.17576/jsm-2019-4801-28
36. Khashi'ie NS, Md Arifin N, Nazar R, et al. A stability analysis for magnetohydrodynamics stagnation point flow with zero nanoparticles flux condition and anisotropic slip. *Energies* 2019; 12(7): 1268. doi: 10.3390/en12071268
37. Khashi'ie NS, Arifin NM, Pop I, et al. Non-axisymmetric Homann stagnation point flow and heat transfer past a stretching/shrinking sheet using hybrid nanofluid. *International Journal of Numerical Methods for Heat & Fluid Flow* 2020; 30(10): 4583–4606. doi: 10.1108/hff-11-2019-0824
38. Khashi'ie NS, Arifin NM, Nazar R, et al. Magnetohydrodynamics (MHD) axisymmetric flow and heat transfer of a hybrid nanofluid past a radially permeable stretching/shrinking sheet with Joule heating. *Chinese Journal of Physics* 2020; 64: 251–263. doi: 10.1016/j.cjph.2019.11.008
39. Srivastava HM, Khan Z, Mohammed PO, et al. Heat transfer of buoyancy and radiation on the free convection boundary layer MHD flow across a stretchable porous sheet. *Energies* 2022; 16(1): 58. doi: 10.3390/en16010058
40. Wang CY. Fluid flow due to a stretching cylinder. *The Physics of Fluids* 1988; 31(3): 466–468. doi: 10.1063/1.866827
41. Butt AS, Ali A, Mehmood A. Numerical investigation of magnetic field effects on entropy generation in viscous flow over a stretching cylinder embedded in a porous medium. *Energy* 2016; 99: 237–249. doi: 10.1016/j.energy.2016.01.067
42. Rehman KU, Al-Mdallal QM, Qaiser A, et al. Finite element examination of hydrodynamic forces in grooved channel having two partially heated circular cylinders. *Case Studies in Thermal Engineering* 2020; 18: 100600. doi: 10.1016/j.csite.2020.100600
43. Abbas Z, Rasool S, Rashidi MM. Heat transfer analysis due to an unsteady stretching/shrinking cylinder with partial slip condition and suction. *Ain Shams Engineering Journal* 2015; 6(3): 939–945. doi: 10.1016/j.asej.2015.01.004
44. Abaszadeh M, Safavinejad A, Amiri H, Amiri Delouei A. A direct-forcing IB-LBM implementation for thermal radiation in irregular geometries. *Journal of Thermal Analysis and Calorimetry* 2022; 147(20): 11169–11181. doi: 10.1007/s10973-022-11328-1
45. Abaszadeh M, Safavinejad A, Amiri Delouei A, Amiri H. Analysis of radiative heat transfer in two-dimensional irregular geometries by developed immersed boundary-lattice Boltzmann method. *Journal of Quantitative Spectroscopy and Radiative Transfer* 2022; 280: 108086. doi: 10.1016/j.jqsrt.2022.108086
46. Atashafrooz M, Sajjadi H, Amiri Delouei A. Simulation of combined convective-radiative heat transfer of hybrid nanofluid flow inside an open trapezoidal enclosure considering the magnetic force impacts. *Journal of Magnetism and Magnetic Materials* 2023; 567: 170354. doi: 10.1016/j.jmmm.2023.170354
47. Al Sakkaf LY, Al-Mdallal QM, Al Khawaja U. A numerical algorithm for solving higher-order nonlinear BVPs with an application on fluid flow over a shrinking permeable infinite long cylinder. *Complexity* 2018; 2018: 1–11. doi: 10.1155/2018/8269541
48. Cunning GM, Davis AMJ, Weidman PD. Radial stagnation flow on a rotating circular cylinder with uniform transpiration. *Journal of Engineering Mathematics* 1998; 33(2): 113–128. doi: 10.1023/A:1004243728777
49. Wan Zaimi WMKA, Ishak A, Pop I. Unsteady viscous flow over a shrinking cylinder. *Journal of King Saud University-Science* 2013; 25(2): 143–148. doi: 10.1016/j.jksus.2012.11.005
50. Waini I, Ishak A, Pop I. Hybrid nanofluid flow towards a stagnation point on a stretching/shrinking cylinder. *Scientific Reports* 2020; 10(1): 9296. doi: 10.1038/s41598-020-66126-2
51. Devi SPA, Devi SSU. Numerical investigation of hydromagnetic hybrid Cu–Al_2O_3/water nanofluid flow over a permeable stretching sheet with suction. *International Journal of Nonlinear Sciences and Numerical Simulation* 2016; 17(5): 249–257. doi: 10.1515/ijnsns-2016-0037
52. Waini I, Ishak A, Pop I. Unsteady flow and heat transfer past a stretching/shrinking sheet in a hybrid nanofluid. *International Journal of Heat and Mass Transfer* 2019; 136: 288–297. doi: 10.1016/j.ijheatmasstransfer.2019.02.101
53. Oztop HF, Abu-Nada E. Numerical study of natural convection in partially heated rectangular enclosures filled with nanofluids. *International Journal of Heat and Fluid Flow* 2008; 29(5): 1326–1336. doi: 10.1016/j.ijheatfluidflow.2008.04.009
54. Liao S. *The Proposed Homotopy Analysis Technique for the Solution of Nonlinear Problems* [PhD thesis]. Shanghai Jiao Tong University; 1992.
55. Li Y, Nohara BT, Liao S. Series solutions of coupled Van der Pol equation by means of homotopy analysis method. *Journal of Mathematical Physics* 2010; 51(6): 063517. doi: 10.1063/1.3445770
56. Liao S. A kind of approximate solution technique which does not depend upon small parameters—II. An application in fluid mechanics. *International Journal of Non-Linear Mechanics* 1997; 32(5): 815–822. doi: 10.1016/S0020-7462(96)00101-1
57. Liao S. On the analytic solution of magnetohydrodynamic flows of non-Newtonian fluids over a stretching sheet. *Journal of Fluid Mechanics* 2003; 488: 189–212. doi: 10.1017/S0022112003004865
58. S. Liao, A new branch of solutions of boundary-layer flows over an impermeable stretched plate. *International*

Journal of Heat and Mass Transfer 2005; 48(12): 2529–2539. doi: 10.1016/j.ijheatmasstransfer.2005.01.005
59. Liao S. An optimal homotopy-analysis approach for strongly nonlinear differential equations. *Communications in Nonlinear Science and Numerical* 2010; 15(8): 2003–2016. doi: 10.1016/j.cnsns.2009.09.002
60. Liao S, Tan Y. A general approach to obtain series solutions of nonlinear differential equations. *Studies in Applied Mathematics* 2007; 119(4): 297–354. doi: 10.1111/j.1467-9590.2007.00387.x